Available online at www.sciencedirect.com
SCIENCE DIRECT®
Physica A 337 (2004) 36–66
PHYSICA A
www.elsevier.com/locate/physa

Stability criteria of the Vlasov equation and quasi-stationary states of the HMF model

Yoshiyuki Y. Yamaguchi[a,b], Julien Barré[c,1], Freddy Bouchet[a,c,d], Thierry Dauxois[c], Stefano Ruffo[a,*]

[a] *Dipartimento di Energetica "S. Stecco" and CSDC, Università di Firenze, INFM and INFN, Via S. Marta, 3 I-50139 Firenze, Italy*
[b] *Department of Applied Mathematics and Physics, Graduate School of Informatics, Kyoto University, 606-8501 Kyoto, Japan*
[c] *Laboratoire de Physique, UMR-CNRS 5672, ENS Lyon, 46 Allée d'Italie, 69364 Lyon Cédex 07, France*
[d] *Dipartimento di Fisica Università "La Sapienza" & INFM Unità di Roma1, P.le A. Moro 2, I-00185 Roma, Italy*

Received 18 September 2003; received in revised form 12 December 2003

Abstract

We perform a detailed study of the relaxation towards equilibrium in the Hamiltonian Mean-Field model, a prototype for long-range interactions in N-particle dynamics. In particular, we point out the role played by the infinity of stationary states of the associated $N \to \infty$ Vlasov dynamics. In this context, we derive a new general criterion for the stability of any spatially homogeneous distribution, and compare its analytical predictions with numerical simulations of the Hamiltonian, finite N, dynamics. We then propose, and verify numerically, a scenario for the relaxation process, relying on the Vlasov equation. When starting from a nonstationary or a Vlasov unstable stationary state, the system shows initially a rapid convergence towards a stable stationary state of the Vlasov equation via nonstationary states: we characterize numerically this dynamical instability in the finite N system by introducing appropriate indicators. This first step of the evolution towards Boltzmann–Gibbs equilibrium is followed by a slow quasi-stationary process, that proceeds through different stable stationary states of the Vlasov equation. If the finite N system is initialized in a Vlasov stable homogeneous state, it remains trapped in a quasi-stationary state for times that increase with the nontrivial power law $N^{1.7}$. Single particle momentum distributions in such a quasi-stationary regime do not have power-law tails, and hence cannot be fitted by the q-exponential distributions derived from Tsallis statistics.

*Corresponding author. Fax: +39-055-4796342.
E-mail addresses: yyama@amp.i.kyoto-u.ac.jp (Y.Y. Yamaguchi), jbarre@cnls.lanl.gov (J. Barré), Freddy.Bouchet@ens-lyon.fr (F. Bouchet), Thierry.Dauxois@ens-lyon.fr (T. Dauxois), ruffo@avanzi.de.unifi.it (S. Ruffo).
[1] Currently at Los Alamos National Laboratory, Theory Division.

0378-4371/$ - see front matter © 2004 Elsevier B.V. All rights reserved.
doi:10.1016/j.physa.2004.01.041

PACS: 05.20. – y; 05.45. – a; 05.70.Ln; 52.65.Ff

Keywords: Hamiltonian dynamics; Long-range interactions; Vlasov equation; Nonlinear stability; Relaxation times

1. Introduction

Relaxation to thermal Boltzmann–Gibbs equilibrium in N-particle Hamiltonian systems with long-range interactions has been recently the subject of an intense debate [1]. In some cases, the relaxation time has been shown to be extremely long and to increase with the number of particles. Hence, the study of these out-of-equilibrium conditions is of paramount importance for physical applications. The dynamics of systems with long-range interactions shows that some states are attained quickly, on time scales of $O(1)$, and that afterwards the system evolves very slowly, on time scales diverging with N, towards Boltzmann–Gibbs equilibrium. We call states that evolve on time scales that diverge with N "quasi-stationary". Some of them are characterized by a particle distribution in the μ-space, $f(\mathbf{r},\mathbf{p},t)=\sum_i^N \delta(\mathbf{r}-\mathbf{r}_i(t),\mathbf{p}-\mathbf{p}_i(t))$ (with $(\mathbf{r}_i,\mathbf{p}_i)$ the position and conjugate momentum of the ith particle and δ the Dirac function), which remains close to a slowly varying smooth distribution for times that increase with N.

It should be remarked that most of the numerical evidences of this behavior are for 1D and 2D systems.[2] The theoretical explanation we propose in this paper, which is developed for mean-field models, extends to any dimension, as soon as the two body interaction is sufficiently smooth. Many recent studies of such quasi-stationary states are performed for the so-called Hamiltonian Mean Field (HMF) model (for a review see Ref. [3]). This model describes the motion of N rotators under the action of an attractive or repulsive infinite range cosine interaction. In this paper we will consider the attractive case. The model then displays a second-order phase transition, which is related to the development of a dynamical instability of the spatially homogeneous initial state with Gaussian distribution of momenta, at a given value of the energy [4].

The analysis developed in this paper is based on a theorem due to Braun and Hepp [5,6], according to which the dynamics of a classical N-particle system interacting via a two body and sufficiently regular long-range potential is well approximated by the associated Vlasov dynamics of the density in μ-space. In the case in which the interaction force derives from a two-body smooth potential, Vlasov equation writes

$$\frac{\partial f}{\partial t}+\mathbf{p}\cdot\nabla_{\mathbf{r}}f-\nabla_{\mathbf{r}}U\cdot\nabla_{\mathbf{p}}f=0\,. \tag{1}$$

The mean field macroscopic potential U is a functional of the probability distribution function $f(\mathbf{r},\mathbf{p},t)$, which makes the equation nonlinear in f. More precisely, Braun–Hepp's theorem states that, for a mean-field microscopic two-body smooth potential, the distance[3] between two initially close "weak" solutions of the Vlasov equation increases

[2] Preliminary indications that it extends to higher dimensions can be found in Ref. [2].

[3] The distance is measured in the Wasserstein metric, defined on the space of all measures.

at most exponentially in time. The theorem applies also to singular distributions, e.g. distributions that have a support on a set of dimension smaller than the one of the μ-space (for instance, a line in the 2D μ-space of the HMF model). If we apply this result to a large N particle approximation of a continuous distribution the error at $t=0$ is typically of order $1/\sqrt{N}$, thus for any "small" ε and any "large enough" particle number N, there is a time t up to which the dynamics of the original Hamiltonian and its Vlasov description coincide within an error bounded by ε. The theorem implies that this time t increases at least as $\ln N$. Extensions to wave particle dynamics of such a result have also been recently reported [7,8]. Since quasi-stationary states evolve on time scales that diverge with N, this result suggests that these states might gain their stability from being "close" to some stable stationary states of the Vlasov dynamics.

Besides the conserved quantities of the Hamiltonian dynamics (energy, momentum, angular momentum, etc.), the Vlasov description introduces additional integrals: the so-called Casimirs

$$C_s[f] = \int s(f(\mathbf{r},\mathbf{p},t))\,\mathrm{d}\mathbf{r}\,\mathrm{d}\mathbf{p} \tag{2}$$

where s is a generic function. These conservation laws are responsible for the existence of an infinity of stable stationary states for the Vlasov dynamics. In this paper, we will argue that the existence of this infinity of stationary states is a possible explanation for the generic existence of quasi-stationary states in the finite N-dynamics.

This interpretation rises the following questions. May one predict the quasi-stationary states that emerge after a complex unstable Vlasov dynamics? Among these stationary states, are there some "statistically preferred" states? What governs the relaxation towards equilibrium of the stationary states, and which is the scaling of the relaxation time with the number of particles? We will address in this paper the first and the third question, while the issues related to the second question will be only briefly mentioned.

Before the slow relaxation phase sets in, a fast evolution takes place on a time scale that is independent of N. This phenomenon is denoted as *violent relaxation* in the astrophysical context [9], and is a consequence of the nonlinear complex dynamics of the Vlasov equation. After this very rapid stage, Vlasov dynamics produces thinner and thinner filamentations of the density f, which lead to an apparent equilibrium described by a coarse grained density function $\bar{f}$. A statistical mechanics interpretation of this process has been proposed: for instance, for an initial two level density function, the equilibrium density is of Fermi–Dirac type [9,10]. Even if this may be already a partial answer to our second question above, we will not address in detail the very delicate point of the convergence of the Vlasov dynamics towards *its* statistical equilibrium in the present paper.

Some authors [11] have advanced a challenging interpretation of the quasi-stationary states, suggesting that they should be true "equilibrium" states, obtained by maximizing the Tsallis [12] entropy of the single particle distribution. We think that a landmark of such an interpretation would be the assessment of the existence of power law tails in the single particle momentum (or energy) distributions. Although we will not enter into a detailed fitting of such distributions using Tsallis q-exponentials, we will present a strong evidence of the absence of power law tails in the single particle momentum

distribution at any stage of the time evolution, for the whole class of initial conditions we investigate in this paper, that are all homogeneous in space (see Section 5.3). For an initial condition in which the particles are concentrated in a point and momentum is uniform in an interval around zero, the authors of Ref. [11] have been able to fit a Tsallis q-exponential to the central part of the momentum distribution, after imposing an arbitrary cut-off to the tails. However, these authors do not exhibit any evidence of existence of power law tails, even for such a special initial state.

Moreover, as mentioned above, our analysis applies also to this initial condition although it does not correspond to a stationary state of the Vlasov equation. At best, Tsallis statistics could describe the quasi-stationary states obtained from such a special initial state, but certainly not all of them, in particular those originated from the large class of homogeneous states that are studied in this paper.

Moreover, the steadily progressing dynamical evolution observed for our class of initial conditions does not show any intermediate "statistically preferred" state. As stated above, the time evolution follows a sequence of stationary Vlasov states until, asymptotically, Boltzmann–Gibbs equilibrium is attained.

It should be however mentioned that the special initial state studied in [11] is very interesting from a dynamical point of view, since it shows long-time correlations that are absent for the homogeneous initial states studied here (see also Ref. [13]). Similar initial states produce fractal structures in the μ-space for a self-gravitating sheet model [14].

As discussed above, Braun–Hepp's theorem suggests that the similarity between Hamiltonian N-particle dynamics and Vlasov dynamics persists for times that increase as $\ln N$. These times are linked with the fastest possible instability of the Vlasov dynamics. For stable solutions, the appropriate timescale is, however, the one associated with the fluctuations of the mean field. In agreement with this theoretical remark, we present in Section 5.3 numerical results that indicate that the persistence of quasi-stationary states is present up to times that are much longer than Braun–Hepp's $\ln N$. This time scale increases as a power law in N with a nontrivial exponent. Similar time scales have been found in gravitational systems. This is the case of Chandrasekhar's "collisional" time scale, which is of order $N/\ln N$ [15]. Although such a time scale is similar to those we find in the HMF model, because it signals the final process of relaxation to Boltzmann–Gibbs equilibrium, its origin in our model is certainly different.

In order to reformulate the timescale hierarchy sketched above, we can expect the following scenario:

(1) An initial and fast evolution, well described for all initial conditions by the Vlasov dynamics, takes place on a timescale independent of the particle number N.
(2) The system is then always trapped close to one of the numerous stable stationary states of the Vlasov equation. This state may be the statistical equilibrium of the Vlasov equation (the most probable state with constraints given by the Vlasov invariants).
(3) The system slowly evolves, on a much longer time scale, due to "collisions", or due to the fluctuations around this Vlasov stationary state. Consequently this time

scale will be a function of N. One can expect that this slow evolution takes place passing through different stable Vlasov stationary states.

(4) Finally, the system reaches a particular Vlasov stable state, corresponding to the Boltzmann–Gibbs equilibrium state.

We will try to give support to this scenario in the remaining of the paper. The plan is the following. We first introduce in Section 2 the Hamiltonian Mean Field model. We will then show in Section 3 that the Vlasov dynamics has an infinity of stationary states and we propose a new general stability criterion for any homogeneous distribution (including non-Boltzmann–Gibbs ones). We will compare these analytical results with numerical simulations of the finite-N Hamiltonian dynamics. The rapid convergence towards a stable stationary state of the Vlasov equation is described in Section 4. In the case of unstable stationary states, we will show that the exponential destabilization may be investigated taking advantage of the existence of unstable modes of the Vlasov dynamics, in accordance with Braun–Hepp's theorem. The slow evolution towards equilibrium, passing through different stable Vlasov stationary states, is described in Section 5.

2. The Hamiltonian Mean Field model

We will consider the HMF model, whose Hamiltonian is

$$H_N = \frac{1}{2}\sum_{j=1}^{N} p_j^2 + \frac{1}{2N}\sum_{j,k=1}^{N} [1 - \cos(\theta_j - \theta_k)] \,, \tag{3}$$

where $\theta_i \in [-\pi, \pi[$ is the position (angle) of the ith particle on a circle and p_i the corresponding momentum. This system can be seen as representing particles moving on a unit circle interacting via an infinite range attractive cosine potential, or as classical XY-rotators with infinite range ferromagnetic couplings [3]. The magnetization, defined as

$$\vec{M}(t) = (M_x, M_y) = \frac{1}{N}\sum_{j=1}^{N} (\cos\theta_j, \sin\theta_j) \,, \tag{4}$$

or more precisely its modulus, $M(t) = \|\vec{M}(t)\| \leqslant 1$, is the main observable that characterizes the dynamical and thermodynamical state of the system.

Its introduction allows to write the canonical equations of motion as follows:

$$\frac{\mathrm{d}\theta_j}{\mathrm{d}t} = p_j \,,$$

$$\frac{\mathrm{d}p_j}{\mathrm{d}t} = -M_x \sin\theta_j + M_y \cos\theta_j \,. \tag{5}$$

Equilibrium statistical mechanics can be derived exactly both in the canonical and in the microcanonical ensembles [16–18]. In the ferromagnetic case, that we consider here, a minimal free energy (maximum entropy) state with a nonvanishing

magnetization appears when lowering temperature T (resp. energy per particle) below $T_c = \frac{1}{2}$ (resp. $U_c = \frac{3}{4}$). A discontinuity at $T_c(U_c)$ in the second derivative of the free energy (entropy) with respect to magnetization signals a second-order phase transition. This transition is between a low-energy phase with particles forming a cluster (rotators pointing towards a preferred direction), and a high-energy phase with particles evenly distributed on the circle (no preferred direction for rotators).

This theoretical result, valid in the $N \to \infty$ limit, is also confirmed by direct numerical simulations of the equations of motion (5), which moreover allow a careful analysis of finite N corrections and give access to the study of nonequilibrium features. It is in this context that, within the energy range $U \in [0.5, U_c]$, a class of initial states has been found that displays an extremely slow relaxation towards Boltzmann–Gibbs equilibrium [11,16,19–22], with a relaxation time that increases with N. Similar phenomena occur for other particle systems with long-range interaction (self-gravitating stars or point vortices [10]). Indeed, in the context of 2D fluid-dynamics [23,24] and plasma physics [24], the existence of an infinity of stationary states is known since a long time.

These slow relaxation processes have recently attracted considerable attention, since the HMF model can be considered as a simple paradigmatic model of long-range interactions, without the two additional difficulties of gravitational dynamics: singularity at short range and particle evaporation. As briefly recalled in the Introduction, Latora et al. [11] have carefully analyzed an initial condition where all particles are located at the same position on the circle (giving initially $M = 1$) and momentum is uniformly distributed over a finite range, symmetrically around zero. The system shows a fast relaxation towards a small magnetization state which persists for an extremely long time, that increases with N. The authors compare the momentum distribution of such a quasi-stationary state with Tsallis distributions, obtaining some convincing fit of the central part of the distribution only after they impose a cut-off to momentum tails. Montemurro and Zanette [25], analyzing the same initial condition, have even criticized the existence of a small magnetization plateau in time, by presenting some numerical evidence that magnetization first evolves towards a minimum, and then take off again towards the higher equilibrium value. We will avoid this controversial point by using the definition of quasi-stationary state given in the Introduction, i.e., we shall call quasi-stationary a state which still evolves, but on a time scale that diverges with N. Hence, macroscopic properties are well defined over a sufficiently wide time span to allow local running time averages, even though the system slowly and continuously evolves towards equilibrium.

At variance with most previous numerical experiments [11,25], we choose here an initial state where the particles are uniformly distributed on the circle (hence M is initially close to zero, $M = O(1/\sqrt{N})$) and momentum has a uniform distribution centered around zero, as above. We make this choice for two reasons: (i) this state is a stationary state of the Vlasov equation, that describes the HMF model in the $N \to \infty$ limit, (ii) the $M = 0$ state plays a relevant role also in the previous numerical experiments [11,25] and we then thought that it is better to start directly from it. Finally, we think that the analysis of the $M = 0$ initial state can also clarify several aspects of the phenomenology of the $M = 1$ initial state used by the authors above.

As explained in the Introduction, we believe that the Vlasov description is a useful and appropriate tool to understand the slow relaxation process. In the following section, we introduce and discuss the Vlasov equation for the HMF model.

3. The Vlasov dynamics of the HMF model

3.1. Introduction

In the continuum limit, that is keeping the volume (here the interval $[-\pi,\pi[$) and the energy per particle fixed as the number of particles $N \to \infty$, the dynamics governed by Eqs. (5) is described by the Vlasov equation. The state of the finite N system can be described by a single particle time-dependent density function:

$$f_d(\theta, p, t) = \frac{1}{N}\sum_{j=1}^{N} \delta(\theta - \theta_j(t), p - p_j(t)) \,, \tag{6}$$

where δ is the Dirac function. When N is large, it is natural to approximate the discrete density f_d by a continuous one $f(\theta, p, t)$. Using this density, also called μ-space distribution, it is possible to rewrite the two components of the magnetization M given by Eq. (4). They read

$$\bar{M}_x[f] \equiv \int f(\theta, p, t)\cos\theta \,\mathrm{d}\theta \,\mathrm{d}p \,, \tag{7}$$

$$\bar{M}_y[f] \equiv \int f(\theta, p, t)\sin\theta \,\mathrm{d}\theta \,\mathrm{d}p \,. \tag{8}$$

Within this approximation, one can write the potential that affects all the particles as

$$V(\theta)[f] = 1 - \bar{M}_x[f]\cos\theta - \bar{M}_y[f]\sin\theta \,. \tag{9}$$

This potential enters the expression of the Vlasov equation

$$\frac{\partial f}{\partial t} + p\frac{\partial f}{\partial \theta} - \frac{\mathrm{d}V}{\mathrm{d}\theta}[f]\frac{\partial f}{\partial p} = 0 \,, \tag{10}$$

which governs the spatiotemporal evolution of the density f. In the remaining of the paper, we will omit the over-bar on M_x and M_y for the sake of simplicity.

It is important to note that the discrete distribution f_d, a sum of Dirac peaks, contains exactly the true dynamics of the system and is also a solution of the Vlasov equation (10). Then, introducing a suitably defined distance on the space of probability measures on $[-\pi,\pi[\times \mathbb{R}$, it is possible to show [5–7] that the distance between two solutions f_1 and f_2 of Eq. (10) grows at most exponentially in time

$$d(f_1(t), f_2(t)) \leqslant d(f_1(0), f_2(0))\mathrm{e}^{\gamma t} \tag{11}$$

with a growth rate γ which is independent of the initial conditions. This result, which is the essence of Braun–Hepp's theorem, heavily relies on the mean field character of

the underlying Hamiltonian dynamics and on the genericity of exponential instability of trajectories. Choosing then $f_1(\theta, p, t) = f_d(\theta, p, t)$ and taking for $f_2(\theta, p, t)$ a continuous approximation of f_d, one immediately obtains that $d(f_1(0), f_2(0)) \to 0$ as N grows. As a consequence, the previous result implies that the discrete particle dynamics converges to Vlasov dynamics when $N \to \infty$, uniformly over all fixed time intervals $[0, T]$. However, for all fixed N there is a typical time $\tau \sim \gamma^{-1}$ over which the two dynamics diverge.

From this analysis, it is therefore natural to expect that particle and Vlasov dynamics coincide during a time that diverges as $\ln N$, if $d(f_d(0), f(0)) \sim 1/N$ and γ is independent of N. However, for initial conditions corresponding to stable stationary solutions of the Vlasov equation, this time may be much longer, actually of order N [26].

All this explains why the properties of the Vlasov equation are of particular interest for the study of the particle dynamics. In the next subsection, we will study the Vlasov dynamics of the HMF model and its stationary states, with the aim of getting useful insights on particle dynamics.

3.2. The Vlasov dynamics and its stationary states

The Vlasov equation inherits from the particle dynamics the conservation of the energy H_V

$$H_V[f] = \int \frac{p^2}{2} f(\theta, p, t)\, \mathrm{d}\theta\, \mathrm{d}p + \frac{1}{2} - \frac{M_x^2 + M_y^2}{2} \tag{12}$$

and of the total momentum

$$P[f] = \int p f(\theta, p, t)\, \mathrm{d}\theta\, \mathrm{d}p\ . \tag{13}$$

However, the Casimir's functionals (2), defined for any continuous function s, yield an infinity of additional conserved quantities, linked with the labeling symmetry when following a fluid particle in the μ-space. These new conserved quantities play of course a major role in the dynamics of the Vlasov equation and thus of particle dynamics.

For a nonstationary initial distribution, the dynamics of the Vlasov equation is known to give rise to a very complex nonlinear evolution, characterized by stretching and folding of the initial distribution, the details of this evolution being usually unpredictable. However, one may predict the final evolution using statistical mechanics arguments, in the spirit of the statistical mechanics of 2D conservative flows [27,28] or of the Vlasov–Poisson equation [29,30]. One ends up with the most probable coarse-grained distribution $\bar{f}$, which takes into account the dynamical invariants. Unfortunately, the dynamical mixing of the distribution is likely to be incomplete: the reason lies in the existence of infinitely many stable stationary solutions of the Vlasov equation, in the neighborhood of which the system may be trapped. Therefore, under Vlasov dynamics an initial state quickly converges (weak convergence) to a stable stationary state which should be studied in detail.

Equations (7) and (8) show that the magnetization $\vec{M}$ is constant for a stationary solution $f(\theta, p)$. This implies that the potential V is constant. The equation for the

stationary states of the Vlasov equation may thus be considered as a linear first-order partial differential equation. Solutions are then given by densities f that are constant on the characteristics of the equation, corresponding to the level sets of the individual particle energy

$$e(\theta, p) = \frac{p^2}{2} + V(\theta) = \frac{p^2}{2} - M_x \cos\theta - M_y \sin\theta \,, \tag{14}$$

which corresponds to the energy of a pendulum. It is important to observe that the total energy H_V given by Eq. (12), is different from the sum of the individual energies (14).

Smooth stationary solutions of the Vlasov equation are thus given by

$$f(\theta, p) = \Phi(e(\theta, p)) \,, \tag{15}$$

where Φ is any real function. Moreover, the values of M_x, M_y and the function Φ must be self-consistent. The Boltzmann–Gibbs equilibrium density

$$f_{eq}(\theta, p) = A \exp(-\beta e(\theta, p)) \tag{16}$$

is a particular case, although very important. One may also prove that stationary states of the Vlasov equation in a moving frame with constant velocity v are given by $f(\theta, p) = \Phi(e(\theta, p) + vp)$.

Let us note that the function Φ may be multi-valued for individual energies e greater than the energy of the separatrix (one branch for particles with positive momentum and the other for negative momenta). We will assume that this does not happen in the remaining of the paper, for the sake of simplicity (a generalization would be straightforward).

3.3. Stability of stationary states of the Vlasov equation

As discussed above, the stationary states of the Vlasov equation are not true stationary states of the particle dynamics. If the former are stable, however, they may explain the long lifetime of quasi-stationary states in the particle dynamics. Linear stability results for the stationary states of the Vlasov equation have been already reported in the case of spatially homogeneous distributions for both Gaussian [4] and water bag [16] momentum distributions. In this section, we will show that it is possible to derive stability results for arbitrary spatially homogeneous stationary states, using a method developed in the context of two 2D fluid dynamics and in plasma physics [24], based on original ideas introduced by Arnold [23].

The authors of Ref. [24] actually study *nonlinear stability*, a concept that we would like to briefly distinguish from other stability concepts. For a generic dynamical system, any extremum f_0 of a conserved quantity $F[f]$ is a stationary point of the dynamics. It is said to be *formally stable* if the second variations $\Delta_2 F[\delta f_1, \delta f_2]$ of F is positive definite (f_0 is then a minimum) or negative definite (f_0 is then a maximum). In the case of the linearized dynamics around a formally stable point f_0, as the second variations of F at f_0 are conserved, a small perturbation of f_0 remains bounded in the norm provided by the second variations: this state is *linearly stable*. Since this implies that

the spectrum of the linearized dynamics does not have any negative value, the system is also *spectrally stable*. It is however not true in general that spectral stability implies linear stability, and that linear stability implies formal stability. Finally, nonlinear stability corresponds to the case where a small perturbation, evolving according to the real dynamics, remains bounded in some norm. It can be shown that nonlinear stability implies spectral stability, the converse being wrong in general, whereas formal stability implies nonlinear stability only in finite dimensional systems.

In this section we prove that any stationary state of the Vlasov equation, defined by Eq. (15) with Φ strictly decreasing, corresponds to a critical point of some invariant functional. Computing the second variations of this functional, we can therefore exhibit a *necessary and sufficient condition of formal stability* for such a stationary state.

Let us consider the maximum of the functional

$$F[f] = C_s[f] - \beta H_V[f] - \mu \int f(\theta, p, t)\, \mathrm{d}\theta\, \mathrm{d}p\ , \tag{17}$$

where H_V is energy (12), C_s is a Casimir functional (2) corresponding to a strictly concave function s and β is positive. Performing the first variations of this functional, we obtain the equation

$$s'(f_0) = \beta \left(\frac{p^2}{2} - \int \cos(\theta - \alpha) f_0(\alpha, p, t)\, \mathrm{d}\alpha\, \mathrm{d}p \right) + \mu = \beta e(\theta, p) + \mu\ , \tag{18}$$

which defines the critical points f_0. This yields

$$f_0(\theta, p) = \Psi(\beta e(\theta, p) + \mu)$$

with e given by (14) and Ψ the inverse function of s', the derivative of s. The condition that s is strictly concave is equivalent to the fact that Ψ is strictly decreasing.

The computation of the second variation of F gives

$$\Delta_2 F[\delta f, \delta f] = \int s''(f_0(\theta, p))[\delta f(\theta, p)]^2\, \mathrm{d}\theta\, \mathrm{d}p + \beta((M_x[\delta f])^2 + (M_y[\delta f])^2)\ , \tag{19}$$

where M_x and M_y are given by Eqs. (7) and (8). As s is strictly concave, s'' is negative. The first term of $\Delta_2 F[\delta f, \delta f]$ is thus clearly negative whereas the second one is positive. We will consider now only homogeneous states, corresponding to $M_x = M_y = 0$ and $f_0(\theta, p) = f_0(p) = \Psi(\beta p^2/2 + \mu)$.

Let us introduce the Fourier series of the perturbation

$$\delta f(\theta, p, t) = \sum_n c_n(p, t) \cos n\theta + s_n(p, t) \sin n\theta\ . \tag{20}$$

From Eq. (19), after integration on the spatial variable θ, one obtains the second variations

$$\Delta_2 F[\delta f, \delta f] = \int s''(f_0(p)) \sum_{n>1} (c_n^2(p) + s_n^2(p))\, \mathrm{d}p + 2G(c_1(p)) + 2G(s_1(p))\ , \tag{21}$$

where we have introduced

$$G(c(p)) \equiv \int s''(f_0(p))c^2(p)\,\mathrm{d}p + \frac{\beta}{2}\left(\int c(p)\,\mathrm{d}p\right)^2 . \tag{22}$$

The terms involving c_n and s_n, $n > 1$, in Eq. (21), are clearly negative definite, since s'' is strictly negative. Consequently, the second variations of F are negative definite if and only if G is negative definite.

The sign of the G function can be studied using the Cauchy–Schwartz inequality:

$$\left(\int c(p)\,\mathrm{d}p\right)^2 = \left(\int \frac{c(p)\sqrt{-s''(f_0(p))}}{\sqrt{-s''(f_0(p))}}\,\mathrm{d}p\right)^2 \tag{23}$$

$$\leqslant \left(\int s''(f_0(p))c^2(p)\,\mathrm{d}p\right)\left(\int \frac{\mathrm{d}p}{s''(f_0(p))}\right) . \tag{24}$$

This inequality leads therefore to

$$G(c(p)) \leqslant \int s''(f_0(p))c^2(p)\,\mathrm{d}p\left(1 + \frac{\beta}{2}\left(\int \frac{1}{s''(f_0(p))}\,\mathrm{d}p\right)\right) . \tag{25}$$

Recalling that s'' is strictly negative, we conclude that if the quantity

$$1 + \frac{\beta}{2}\int \frac{\mathrm{d}p}{s''(f_0(p))} \tag{26}$$

is positive, the function G is negative. Conversely, when it is negative, considering the particular function $c(p) = -1/s''(f_0(p))$ demonstrates that G may be positive.

Differentiating with respect to the variable p the equality

$$s'(f_0(p)) = \beta\frac{p^2}{2} + \mu \tag{27}$$

obtained from Eq. (18) in the case of homogeneous states, yields

$$\frac{\beta}{s''(f_0(p))} = \frac{f_0'(p)}{p} . \tag{28}$$

As $f_0'(0) = 0$, quantity (26) can be written as

$$I[f_0] = 1 + \frac{1}{2}\int_{-\infty}^{+\infty} \frac{f_0'(p)}{p}\,\mathrm{d}p . \tag{29}$$

This leads to the following equivalence:

$$f_0 \text{ is formally stable } \Leftrightarrow\ I[f_0] > 0 . \tag{30}$$

This condition will be of course an excellent criterion to predict the stability of several initial conditions, and therefore the lifetime of the corresponding quasi-stationary states. This is what we will consider now.

Let us note that Inagaki and Konishi [31] have found a dispersion relation for the linearized Vlasov equation which leads to the above stability criterion. Hence, in this particular case, linear stability and formal stability criteria coincide.

3.4. Applications of the nonlinear stability criteria

Waterbag distribution: One of the most widely used initial condition in previous numerical studies of the HMF model is the so-called waterbag distribution:

$$f_{wb}(p) = \begin{cases} 0 & \text{if } |p| > \bar{p}\,, \\ 1/(2\bar{p}) & \text{if } -\bar{p} < p < \bar{p}\,. \end{cases} \tag{31}$$

If $M_x = M_y = 0$ (homogeneous state), the relation between energy $H_V = U$ and $\bar{p}$ is $\bar{p} = \sqrt{6U - 3}$. Computing the first derivative of f_{wb}

$$f'_{wb}(p) = \frac{1}{2\bar{p}}\left[\delta(p + \bar{p}) - \delta(p - \bar{p})\right], \tag{32}$$

one obtains the following expression:

$$I[f_{wb}] = 1 - \frac{1}{2}\,\frac{1}{\bar{p}^2}\,, \tag{33}$$

exhibiting that the critical width of the distribution, above which the waterbag is formally unstable, is $\bar{p}_c = 1/\sqrt{2}$. This corresponds to the critical energy density

$$U_c^* = \tfrac{7}{12} \tag{34}$$

as reported earlier [16].

Gaussian distribution: As a second example, let us consider a Gaussian distribution:

$$f_g(p) = \sqrt{\frac{\beta}{2\pi}}\,\mathrm{e}^{-\beta p^2/2} \tag{35}$$

characteristic of an equilibrium canonical distribution. In this case, the quantity in Eq. (29) can be easily reduced to

$$I[f_g] = 1 - \frac{\beta}{2} \tag{36}$$

emphasizing that the critical inverse temperature is $\beta_c^* = 2$ and consequently the critical energy density $U_c^* = \frac{3}{4}$. This coincides with the critical point of the second-order phase transition U_c.

Mixed distribution: Finally, let us consider a more general distribution, namely a mixed distribution between f_{wb} and f_g, defined as

$$f_a(p) = (1 - a) f_{wb}(p) + a f_g(p)\,. \tag{37}$$

Thanks to the linearity of quantity (29) with respect to the distribution, the critical energy density for this mixed distribution f_a is obtained as a linear combination of

both previous results:

$$U_c^*(a) = \frac{7}{12}(1-a) + \frac{3}{4}a = \frac{7}{12} + \frac{a}{6}\,. \tag{38}$$

Such a result allows to define a phase diagram of the dynamical critical energy that we will be able to confirm using numerical simulations. We aim in the following at showing how these considerations about the Vlasov equation and its stationary states are useful to understand the dynamics of the discrete particle system. We begin in Section 4 by studying the short time evolution, and turn in Section 5 to the intermediate and long time behavior.

4. Short time behavior

4.1. The numerical setup

We have numerically integrated the canonical equations of motion (5), by using symplectic fourth-order integrators, the McLachlan–Atela's [32] or Yoshida's [33] algorithms. The timestep $\mathrm{d}t = 0.1$ was chosen to obtain an energy conservation with a relative accuracy $|\Delta E/E|$ better than 10^{-7}. We will consider initial conditions with uniform distribution with respect to θ as explained in Section 3.3. The magnetization being consequently zero, these states are stationary solutions of the Vlasov equation (10).

However, the numerical calculations correspond to simulations with a *finite* number of degrees of freedom, and these initial states are not anymore stationary a priori. The spatial coordinates θ_j are randomly chosen in the interval $[-\pi, \pi[$, which leads to a magnetization of order $1/\sqrt{N}$ initially. The momenta p_j are also randomly chosen from the given distribution $f(p)$ satisfying the conditions for the energy:

$$\frac{1}{N}\sum_{j=1}^{N}\frac{p_j^2}{2} = U - \frac{1}{2}\,, \tag{39}$$

whereas the conserved total momentum is set to zero:

$$\sum_{j=1}^{N} p_j = 0\,. \tag{40}$$

We will present how the numerical results allow us to detect the critical energy for dynamical instability, using first the most widely used initial conditions, the waterbag distribution, and then the mixed ones.

4.2. Waterbag initial distributions

4.2.1. The first peak of the magnetization

Figure 1 presents the initial temporal evolution of the magnetization $M(t)$ for different values of the energy density, but with the same number of particles, for a system

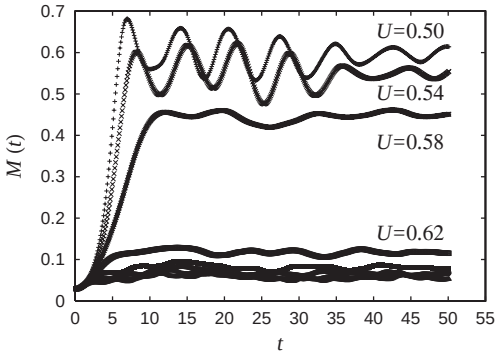

Fig. 1. Temporal evolution of $M(t)$ for different values of the energy density U, when the number of particles is $N = 10^3$. The values of U are from 0.50 to 0.78 with 0.04 step size. The curves correspond to averages over 100 samples.

initialized with a waterbag distribution in momentum and a homogeneous one for the angles (M is close to zero since initially $M = O(1/\sqrt{N})$). Averages over a set of initial conditions (samples) are taken. These results (already partially reported elsewhere [34]) show that the initial time evolution of the magnetization, starting from such a nonequilibrium initial condition, is quite different, depending on whether U is larger or smaller than $U_c^* \approx 0.583$. If $U > U_c^*$, but still below the second-order phase transition energy U_c, the magnetization remains close to the $M=0$ initial value and does not show any tendency towards the nonvanishing equilibrium value (the long time relaxation to equilibrium will be discussed in Section 5.3). For $U < U_c^*$, instead, the magnetization shows a fast relaxation to a non vanishing value which is close to equilibrium. Relaxation proceeds through repeated oscillations that damp after a relatively short time. In order to characterize quantitatively this behavior, let us focus on the first peak of $M(t)$, by studying its height and its time of occurrence as a function of the energy density U, as presented in Figure 2 for increasing particle numbers.

Figure 2(a) emphasizes that the first peak height vanishes in the energy region above U_c^* as N increases, in agreement with the theoretical predictions of the Vlasov equation, which imply that the $M = 0$ state becomes stable in this energy range in the continuum ($N \to \infty$) limit. The initial fluctuations of the magnetization, which are of order $1/\sqrt{N}$, do not grow when $U > U_c^*$, because the waterbag state is Vlasov stable. On the contrary, these fluctuations rapidly grow for $U < U_c^*$, leading in a short time to a nonvanishing magnetization state which is close to equilibrium.

Similar indications come from the first peak time, shown in Fig. 2(b). For $U > U_c^*$ this quantity clearly shows a convergence to an asymptotic value as N increases, but this value sharply increases as one approaches U_c^* from above, signaling the instability of the $M = 0$ initial state. The behavior below U_c^* is less clear since the first peak time does not yet show the saturation expected on the basis of the Vlasov equation for the values of N considered here. This might perhaps be due to the limited validity in time of the Vlasov description when starting from an initially unstable state. We will

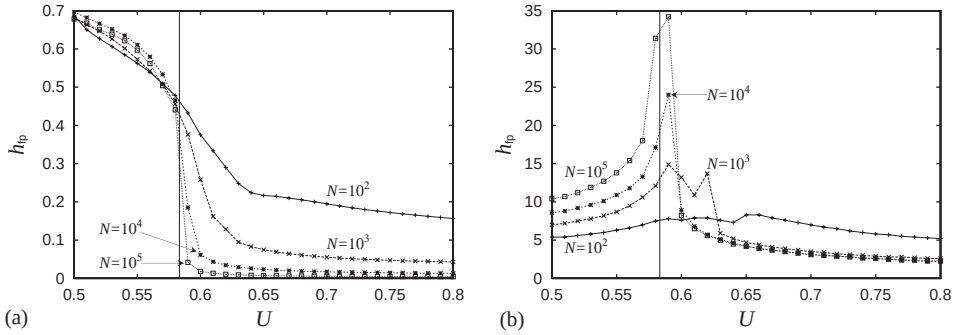

Fig. 2. The first peak height (a) and the first peak time (b) vs. energy density U. The curves correspond to different particle numbers $N = 10^2, 10^3, 10^4$ and 10^5 from top to bottom for $U > U_c^*$ for panel (a) and from bottom to top for $U < U_c^*$ for panel (b), keeping in mind that every curve is obtained averaging over 100 (resp. 20) samples for $N \leqslant 10^4$ (resp. $N = 10^5$). The vertical line represents the theoretical critical energy density U_c^*, given by Eq. (34).

however show in the next section that at least the early exponential instability is well reproduced.

Both quantities, the first peak height and the first peak time, are therefore useful indicators of the presence of a dynamical critical energy U_c^*, as predicted theoretically in the continuum limit. To summarize, we could say that on a $O(1)$ time scale, and when starting from such a waterbag initial state, one would observe the instability of the $M = 0$ state at U_c^* instead of U_c, the phase transition energy.

Before extending these findings to other types of initial distributions in Section 4.3, we will first show in the next section that the predictions of the Vlasov equation are sufficiently precise to give the growth rate of the instability.

4.2.2. *Theoretical estimate of the growth rate*

As shown in Fig. 2(b), a typical time scale of the system (the one of the first peak in magnetization) shows a tendency to diverge at U_c^*. We show in this section that Vlasov equation not only predicts this divergence, but is also quantitative in determining the time scale of the initial exponential instability of the magnetization for $U < U_c^*$.

Let us therefore define the exponential growth rate λ of an initial perturbation $\delta f(\theta, p, 0)$ of a Vlasov stationary unstable state as follows:

$$\|\delta f(\theta, p, t)\| \sim \exp(\lambda t)\ \|\delta f(\theta, p, 0)\|\ . \tag{41}$$

The perturbation we consider is around a homogeneous state, whose density function f depends only on the variable p. However, the perturbation δf depends on all variables (θ, p, t).

The linearized equation that governs the time evolution of the perturbation δf, for vanishing magnetization, is

$$\frac{\partial \delta f}{\partial t} + p\,\frac{\partial \delta f}{\partial \theta} - (\sin\theta M_x[\delta f] - \cos\theta M_y[\delta f])\frac{\partial f}{\partial p} = 0\,. \tag{42}$$

Using the development in Fourier series of the perturbation δf given in Eq. (20), we obtain the following equations for each Fourier component:

$$\frac{\partial c_n}{\partial t} = -nps_n \quad \forall n > 1\,, \tag{43}$$

$$\frac{\partial s_n}{\partial t} = npc_n \quad \forall n > 1\,, \tag{44}$$

$$\frac{\partial c_1}{\partial t} = -ps_1 - \frac{1}{4}\frac{\partial f}{\partial p}\int \mathrm{d}u\; s_1(u,t)\,, \tag{45}$$

$$\frac{\partial s_1}{\partial t} = pc_1 + \frac{1}{4}\frac{\partial f}{\partial p}\int \mathrm{d}u\; c_1(u,t)\,. \tag{46}$$

One can easily show that the Fourier components with $n > 1$ cannot be unstable. Indeed, by introducing the quantity $v_n = c_n + \mathrm{i}s_n$, it is straightforward to show that its time derivative is $v_n' = \mathrm{i}\,pnv_n$. Hence, the generalized eigenvalues are all pure imaginary numbers, $\mathrm{i}np$ (with $p \in \mathbb{R}$), and the corresponding eigenvectors are Dirac delta functions.

Let us then concentrate on the $n=1$ components for waterbag initial conditions. Using expressions (32) for the derivative with respect to p of distribution (31), Eqs. (45) and (46) become

$$\frac{\partial c_1}{\partial t} = -ps_1 - \frac{1}{8\bar{p}}[\delta(p+\bar{p}) - \delta(p-\bar{p})]\int \mathrm{d}u\, s_1(u,t)\,, \tag{47}$$

$$\frac{\partial s_1}{\partial t} = pc_1 + \frac{1}{8\bar{p}}[\delta(p+\bar{p}) - \delta(p-\bar{p})]\int \mathrm{d}u\, c_1(u,t)\,. \tag{48}$$

To solve this infinite dimensional eigenvalue problem, we restrict to functions c_1 and s_1 that are linear combinations of $\delta(p+\bar{p})$ and $\delta(p-\bar{p})$. This yields a 4D problem, whose eigenvalues can be calculated explicitly as functions of $\bar{p}$, and therefore as functions of the energy per particle U.

One finds that above $U_c^* = \frac{7}{12}$ all eigenvalues are pure imaginary, indicating that the Vlasov equation is linearly stable for such perturbations, in full agreement with the stability analysis developed in Section 3.4. Below U_c^*, the largest eigenvalue λ that controls the growth rate is

$$\lambda = \sqrt{6(U_c^* - U)}\,. \tag{49}$$

The exponential growth of perturbations of the initial distribution implies an exponential growth of magnetization $M(t)$. This is indeed confirmed in Fig. 3(a) where the

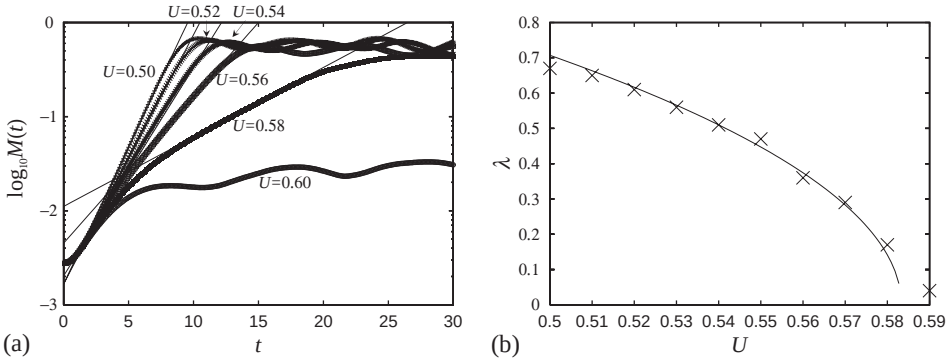

Fig. 3. (a) Semi-log plot of the magnetization $M(t)$ for $N = 10^5$ particles, the number of samples being 20. The values of U are from 0.50 to 0.60 from top to bottom with 0.02 step size. The exponential growth rates of $M(t)$, λ, are estimated from the fitting solid lines. (b) Comparison of the theoretical (solid curve) and numerical (crosses) growth rate λ.

magnetization is plotted versus time in semi-logarithmic scale. The comparison of the theoretical estimate (49) of the growth rate with the numerical results, reported in Fig. 3(b), shows a very good agreement. Moreover, the time scale $1/\lambda$ diverges at U_c^*.

4.3. Extended initial distribution

We present in this section the numerical results for the mixed distributions in formula (37) using the indicators introduced in Section 4.2.1.

The first peak height, shown in Fig. 4, shows a dependence on U which is perfectly consistent with the theoretical prediction of the existence of a critical energy density $U_c^*(a)$, given in formula (38), above which the $M = 0$ state is stable.

However, the numerical results emphasize that the transition is much less abrupt for nonvanishing values of the parameter a than for $a = 0$ (the waterbag case previously analyzed). The explanation of this effect is possibly twofold. On one hand, the stability criterion derived in Section 3.3 gives no information on the time evolution that begins from an unstable initial state: it may well be that the system evolves initially to states with smaller magnetization than for $a = 0$. On the other hand, this weaker instability below U_c^* may be also due to the linear vanishing of the growth rate at U_c^* characteristic of the Gaussian initial distribution [4], instead of the sharper square root behavior of the waterbag initial distribution, as expressed by Eq. (49).

The first peak time data, presented in Fig. 5 as a function of the energy density U, do not follow sometimes a smooth curve. This may be due to the fact that magnetization $M(t)$ is almost flat in the region $U \sim U_c^*$, and hence the first peak time is strongly affected by slight variations in the shape of the function $M(t)$. Nevertheless, the behavior of the first peak time is qualitatively the same as the one shown in Fig. 2(b) for $a = 0$. The same comments made there apply also to this case.

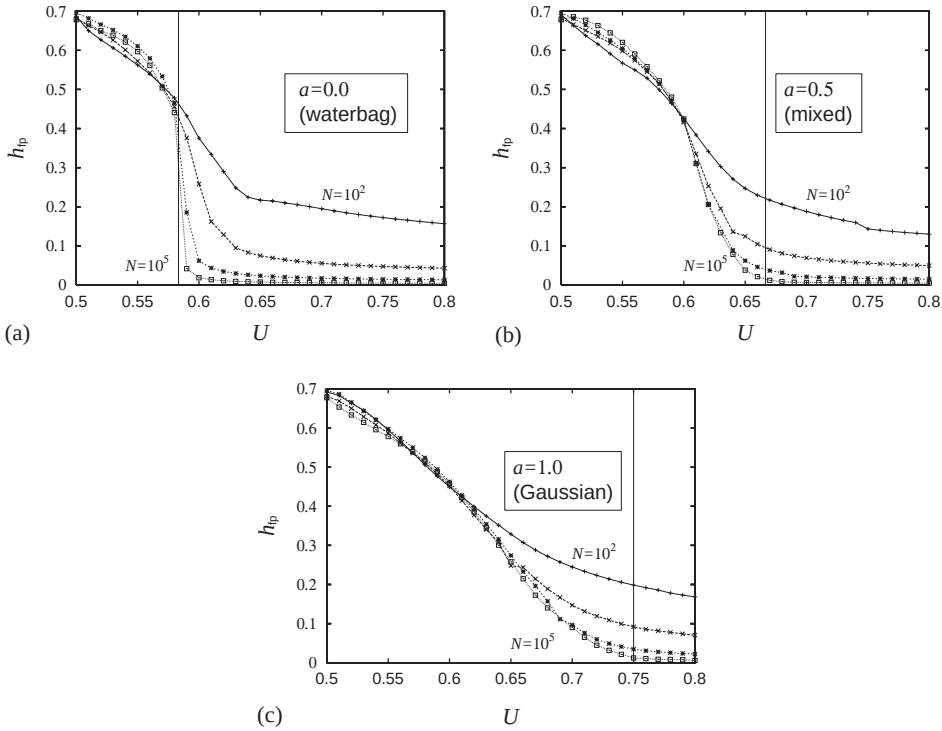

Fig. 4. The first peak heights vs. the energy density U for waterbag (panel (a)), mixed with $a = 0.5$ (panel (b)) and Gaussian (panel (c)) initial conditions. The vertical line represents the theoretical critical energy density $U_c^*(a)$, given by Eq. (38). The different curves correspond to the following values of N: 10^2, 10^3, 10^4 and 10^5 from top to bottom for $U > U_c^*(a)$.

We have shown in this section that the *formal stability* criterion of Vlasov stationary states, stated in Section 3.3, allows to characterize the short time ($O(1)$ time scale) behavior of the finite N dynamics of the HMF model in the $N \to \infty$ limit. In particular, it describes the behavior of the magnetization as a function of the energy per particle U and the presence of several different instability thresholds depending on the detailed properties of the chosen initial distribution. The critical energy for the instability of the Gaussian distribution coincides with the thermodynamical phase transition point U_c, as already remarked by Inagaki [4]. Moreover, the linear stability analysis of the Vlasov equation gives results for the growth rates of the instability that are perfectly confirmed by numerical simulations. Several aspects remain to be ascertained. An important one concerns the intermediate and long time evolution of an initial Vlasov unstable state. In the following section, after introducing suitable indicators of stationarity, we will follow the time evolution of such states for the HMF model. A further important question is the ultimate fate of Vlasov stable $M = 0$ states for the finite N dynamics of the HMF model. In the next section, we will show that these states display indeed a much slower "instability", that becomes evident on a time scale that increases with a

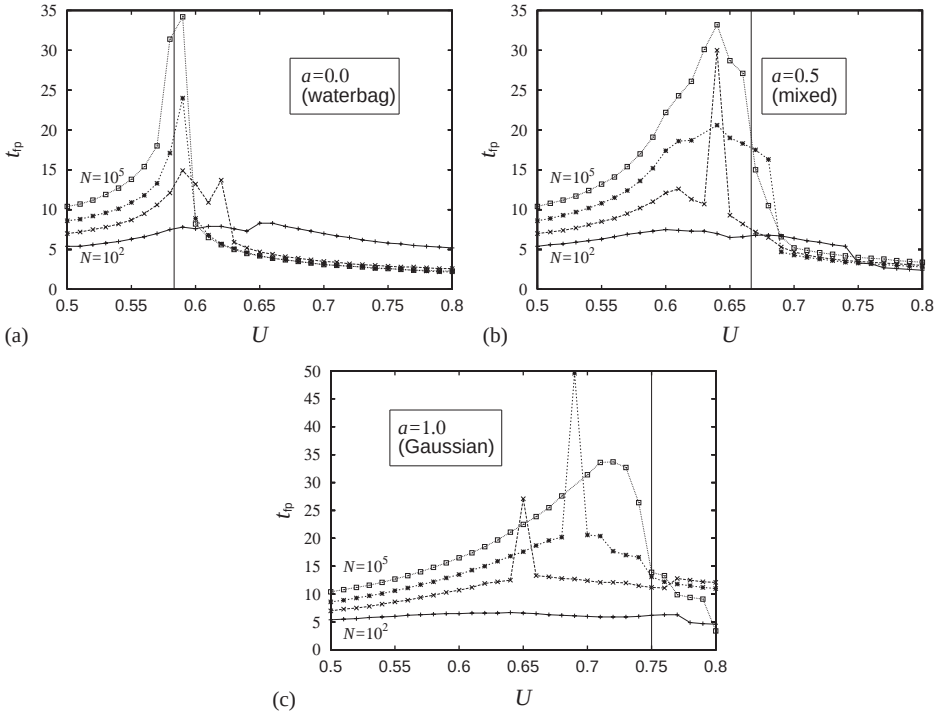

Fig. 5. The first peak time vs. the energy density U for waterbag (panel (a)), mixed (panel (b)) and Gaussian (panel (c)) initial conditions. The vertical line represents the theoretical critical energy density $U_c^*(a)$, given by Eq. (38). The different curves correspond to the following values of N: 10^2, 10^3, 10^4 and 10^5 from bottom to top in $U < U_c^*(a)$.

nontrivial power law in N. These are examples of the *quasi-stationary* states that are the main object of study of this paper.

5. Intermediate and long time behaviors

This section is devoted to the study of the intermediate and long time evolution of both initially unstable and stable Vlasov stationary states. As discussed in the previous section, the initial evolution is well described by Vlasov dynamics. Unstable states quickly evolve (on times of order 1), until they approach, and are trapped, close to stationary states of the Vlasov equation. The system then evolves slowly through these stationary states, until it reaches Boltzmann–Gibbs statistical equilibrium. In this section, we will construct indicators to assess if a N particle state is close to a stationary state (necessary conditions). Using these indicators, we will show that in all cases, during the relaxation towards equilibrium, the system always remains close to Vlasov stationary states.

5.1. Necessary conditions of stationarity

In order to check these features, we need to introduce necessary conditions for stationarity, and to perform numerical tests of nonstationarity for the HMF model. The tests guarantee nonstationarity only, they do not guarantee stationarity. In order to obtain supporting evidences of stationarity, we introduce several indicators of nonstationarity and observe whether all of them fail. We take this fact as a good indication of stationarity.

5.1.1. Energy distribution

If $f_{st}(\theta, p)$ is stationary, so will be the single particle energy distribution, $f_e(e)$. This implies the stationarity of its moments

$$\langle e^j \rangle = \int_0^\infty e^j f_e(e)\,\mathrm{d}e \quad \text{with } j \in \mathbb{N}\ . \tag{50}$$

The logical implications

$$f(\theta, p, t) \text{ stationary} \Rightarrow f_e(e, t) \text{ stationary} \Rightarrow \langle e^j \rangle(t) \text{ stationary} \tag{51}$$

guarantees that the stationarity of the energy moments is a necessary condition for the stationarity of the distribution $f(\theta, p, t)$.

In other words, the system is not stationary if at least one of the moments $\langle e^j \rangle(t)$ is not. The computation of the time derivatives $\mathrm{d}\langle e^j \rangle/\mathrm{d}t$ for the first four moments will be our Test I for nonstationarity.

5.1.2. Symmetry with respect to the spatial variable θ

The previous necessary condition (51) is valid for all Hamiltonian models. It is possible to derive, using symmetry arguments, another necessary condition which is specific of the HMF model. Indeed, using the individual particle energy (14), the Vlasov equation (10) for a stationary distribution can be written as

$$\left[\frac{\partial e}{\partial p}\frac{\partial}{\partial \theta} - \frac{\partial e}{\partial \theta}\frac{\partial}{\partial p}\right] f_{st}(\theta, p) = 0\ . \tag{52}$$

The solution of Eq. (52) is constant on the characteristic curves $e(\theta, p) = \text{constant}$. Moreover, if one always resets to zero the phase of the magnetization vector $\vec{M}(t)$ (i.e., $M_y(t) = 0$), all characteristic curves will be symmetric with respect to a sign reversal of θ. Hence, if f is stationary and the previous condition on the phase of $\vec{M}(t)$ is respected, then the stationary distribution obeys the following symmetry condition:

$$f_{st}(\theta, p) = f_{st}(-\theta, p) \quad \forall p\ . \tag{53}$$

Consequently, an asymmetry of the distribution $f(\theta, p, t)$ with respect to the spatial variable θ, implies that the system is nonstationary.

It is important to note that the symmetry with respect to sign changes in momentum p, $f(\theta, p, t) = f(\theta, -p, t)$, is not a necessary consequence of the stationarity of f.

Two separate characteristic curves for $e > e_s$, where e_s is energy of the separatrix, may correspond to different values of f since they are *not* connected. This symmetry is therefore not required even if the system is stationary. A violation of this symmetry is not therefore an acceptable test of nonstationarity.

Obtaining the distribution $f(\theta, p, t)$ numerically is, however, not easy since it is defined on the 2D μ-space at all fixed times t, and therefore a huge number of samples would be necessary to obtain a good statistics. A trick to easily check asymmetries in $f(\theta, p, t)$ would be to verify the associated symmetry of the marginal distribution function

$$\tilde{f}(\theta, t) = \int f(\theta, p, t)\, \mathrm{d}p \,. \tag{54}$$

However, unfortunately, $\tilde{f}(\theta, t)$ may be symmetric even if symmetry (53) is not satisfied. Typical examples of asymmetric distributions $f(\theta, p, t)$ and corresponding symmetric marginal distributions $\tilde{f}(\theta, t)$ are shown in Figs. 6(a) and (c), respectively. In order to recognize the asymmetry of $f(\theta, p, t)$ with respect to θ, one must consider partially integrated distributions:

$$\tilde{f}_{+}(\theta, t) = \int_{p>0} f(\theta, p, t)\, \mathrm{d}p \quad \text{and} \quad \tilde{f}_{-}(\theta, t) = \int_{p<0} f(\theta, p, t)\, \mathrm{d}p \,. \tag{55}$$

These latter distributions, besides being symmetric if the system is stationary, are able to correctly detect the asymmetries of 2D distributions in (θ, p), as shown in Figs. 6(a) and (c).

We quantitatively observe the time evolution of the asymmetry by introducing the two following quantities:

$$\begin{aligned} A_{+}(t) &= \int [\tilde{f}_{+}(\theta, t) - \tilde{f}_{+}(-\theta, t)]^2\, \mathrm{d}\theta \\ &= \int \mathrm{d}\theta \left[\int_{p>0} \mathrm{d}p (f(\theta, p, t) - f(-\theta, p, t)) \right]^2 , \\ A_{-}(t) &= \int [\tilde{f}_{-}(\theta, t) - \tilde{f}_{-}(-\theta, t)]^2\, \mathrm{d}\theta \\ &= \int \mathrm{d}\theta \left[\int_{p<0} \mathrm{d}p (f(\theta, p, t) - f(-\theta, p, t)) \right]^2 . \end{aligned} \tag{56}$$

Both A_{+} and A_{-} exactly vanish when the distribution is symmetric, but they are affected by numerical errors and finite N effects when estimated from numerical simulations. In order to reduce such effects, we first define the quantity

$$A(t) = \int \mathrm{d}\theta \left[\int \mathrm{d}p (f(\theta, p, t) - f(-\theta, -p, t)) \right]^2 . \tag{57}$$

For initial conditions that are symmetric under the transformation $(\theta, p) \to (-\theta, -p)$, since this symmetry is conserved during the time evolution, $A(t) = 0$ for both stationary or nonstationary distributions. Of course, also this quantity is affected by numerical errors. To factor out such errors, we introduce the quantities $A_{+}(t)/A(t)$ and $A_{-}(t)/A(t)$,

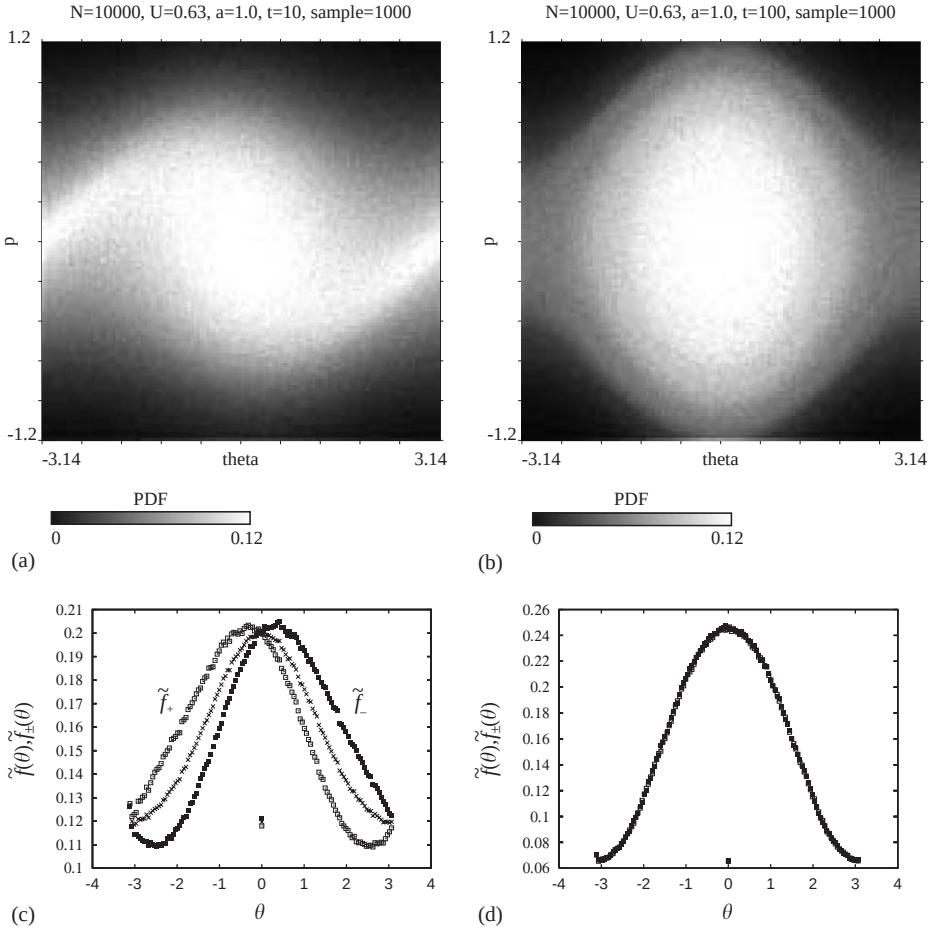

Fig. 6. Typical asymmetric (a) and symmetric (b) distribution $f(\theta, p, t)$. Panel (c) (resp. (d)) presents the marginal distributions $\tilde{f}(\theta, t)$ (crosses), $\tilde{f}_+(\theta, t)$ (open squares) and $\tilde{f}_-(\theta, t)$ (full squares) for the distributions plotted in panel (a) (resp. (b)). The three curves superpose almost perfectly in panel (d). $N = 10^4$, $U = 0.63$, $a = 1.0$, the number of samples is 10^3. Time is $t = 10$ for panels (a) and (c), and $t = 10^2$ for panels (b) and (d).

which are large for asymmetric distributions similar to those in Fig. 6(a), and are instead $O(1)$ for symmetric distributions (actual values taken for the cases shown Fig. 6 are 160 for Fig. 6(a) and 0.4 for Fig. 6(b)). Large values of the quantities $A_\pm/A$ will be our Test II for nonstationarity.

5.2. Nonstationarity test

Now that we have defined these two indicators, let us check nonstationarity by considering both Vlasov unstable and Vlasov stable initial states with waterbag

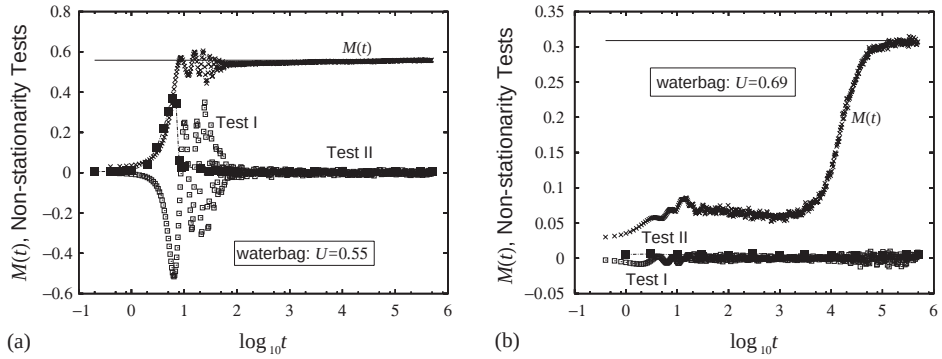

Fig. 7. Nonstationarity tests for a waterbag initial condition with $N = 10^3$ particles and 10^2 samples. Note the logarithmic scale for the time variable. Panels (a) (resp. (b)) presents the time evolution of the magnetization $M(t)$ (crosses), Test I $\mathrm{d}\langle e\rangle/\mathrm{d}t$ (open squares) and Test II $A_+(t)/A(t)$ (full squares) in the unstable case $U = 0.55$ (resp. stable case $U = 0.69$). The quantities $\mathrm{d}\langle e^j\rangle/\mathrm{d}t$ (resp. $A_\pm(t)/A(t)$) are multiplied by a factor 10 (resp. 10^{-2}) for graphical purposes. The horizontal line represents the canonical value of M.

distribution, $a = 0$ in Eq. (37). Typical results of Test-I and-II are shown in Fig. 7.

For Vlasov unstable cases (Fig. 7(a)), the quantity $\mathrm{d}\langle e^j\rangle/\mathrm{d}t$ takes large values only in the time region $2 < t < 80$. Similarly, the indicator $A_\pm(t)/A(t)$ is large in the time region $1 < t < 10$. We have reported only $\mathrm{d}\langle e\rangle/\mathrm{d}t$ and $A_+(t)/A(t)$, but we have checked that the behavior is totally identical for higher moments $j = 2$, 3 and 4 and for $A_-(t)/A(t)$, respectively. This time region of nonstationarity perfectly coincides with the region where the magnetization $M(t)$ rapidly grows or largely fluctuates. For Vlasov stable cases, $\mathrm{d}\langle e^j\rangle/\mathrm{d}t$ exhibits small fluctuations only in the time interval $1 < t < 20$, while $A_\pm(t)/A(t)$ remains small all the time. We guess that the fluctuations in $\mathrm{d}\langle e^j\rangle/\mathrm{d}t$ are due to finite size effects and would vanish in the $N \to \infty$ limit. Note the logarithmic scale for the horizontal time axis: the increase in $M(t)$ in Fig. 7(b) is much slower than the one in Fig. 7(a).

The behavior shown in Fig. 7(b) is very important, because it shows that a variation in M is compatible with the fact that the distribution f may remain stationary; i.e., the system can relax to equilibrium (notably in the time region $[10^4, 10^5]$ in Fig. 7(b)) passing through stationary states of the Vlasov equation. It is natural to suppose in addition that these stationary states are stable.

Figure 8 reports results for two unstable Gaussian initial conditions, $a = 1$ in Eq. (37) with $U = 0.55$ and 0.69. The behavior in panel (a) is very similar to the unstable waterbag case of Fig. 7(a). The case in panel (b) exhibits a small peak around $t = 5$ for both Tests I and II. This presumably indicates that the system is weakly nonstationary at this time, meaning that the temporal variations of the distributions f are small. It is also possible to explain the weakness of the nonstationarity for Gaussian initial conditions with the same arguments that we used when commenting on Fig. 4. This state is unstable below the critical energy $U_c = 0.75$, but the equilibrium

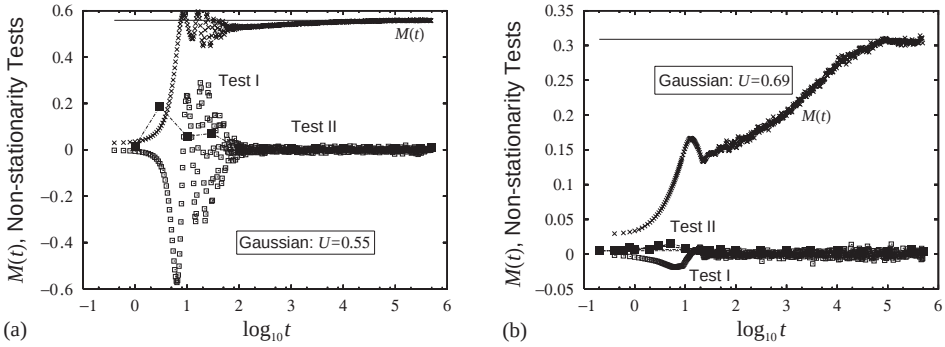

Fig. 8. (a,b) Same plots as in Figs. 7, for a Gaussian initial condition.

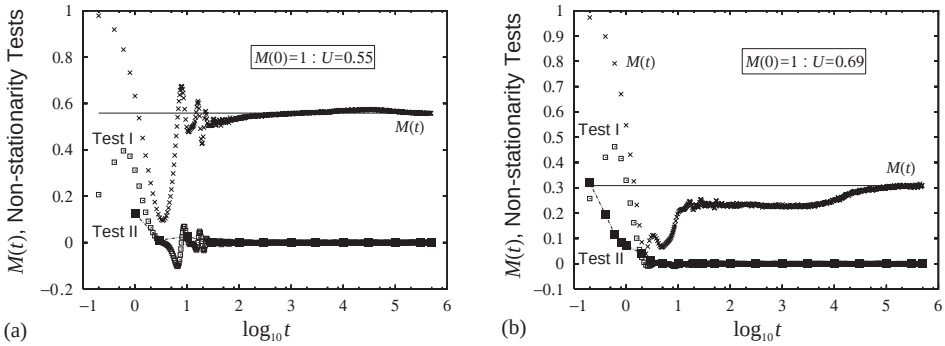

Fig. 9. (a,b) Same plots as in Figs. 7, for waterbag initial conditions in momentum p whereas all the phases θ_j are set at 0, i.e., $M(0)=1$. The quantity $A_+(t)/A(t)$ is multiplied by 10^{-4} for graphical purposes.

value for M goes to zero when U tends to U_c. Hence, the initially unstable state may be very close to stationary stable states, and can be therefore immediately trapped into a stable state. We expect the nonstationarity to become weaker and weaker as U approaches U_c.

The initial conditions used above correspond to stationary solutions of the Vlasov equation. What happens with nonstationary initial conditions? On the basis of what we have found above, we expect that the system reaches a stationary stable state, just like it does when starting from initially unstable stationary states (Figs. 7 and 8). To confirm this expectation, we have prepared the initial condition $M(0)=1$, and we have reported the results of Tests I and II in Fig. 9. In the short time region $t<3$, both $\mathrm{d}\langle e^j\rangle/\mathrm{d}t$ and $A_\pm$ are large but they vanish for longer times, indicating that the system reaches some stationary state of the Vlasov equation.

Summarizing the results of this section, we have found a strong support to the guess that, generically, the states corresponding to stationary stable solutions of the Vlasov equation *attract* stationary unstable and nonstationary solutions. The system

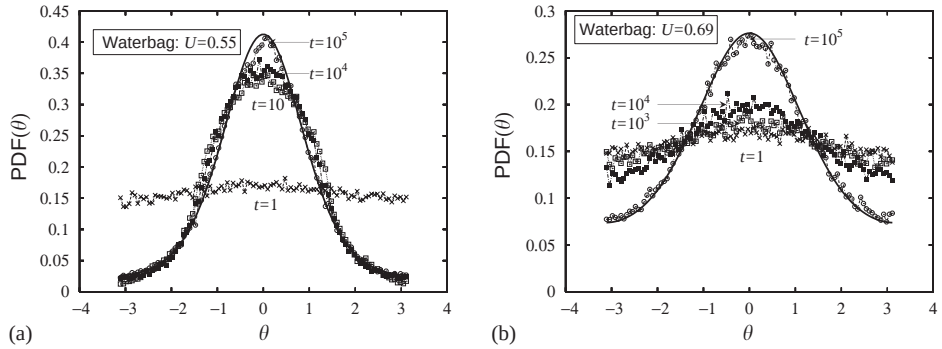

Fig. 10. Temporal evolution of the probability distribution function $\tilde{f}(\theta,t)$ for a waterbag initial condition, identical to the one used for Fig. 7. $N=10^3$ and the number of samples is 10^2. The distributions at times $t=1$ (crosses), $t=10$ (open squares), $t=10^4$ (full squares), $t=10^5$ (open circles), are reported for $U=0.55$ (a), and at $t=1$ (crosses), $t=10^3$ (open squares), $t=10^4$ (full squares), $t=10^5$ (open circles), for $U=0.69$ (b). The solid curve represents the equilibrium distribution, $\exp[M\cos\theta/T]/C$, where $M=0.558$, $T=0.412$ and $C=9.52$ for $U=0.55$ and $M=0.309$, $T=0.475$ and $C=6.97$ for $U=0.69$.

evolves in time passing through a series of stationary solutions of the Vlasov equation.

5.3. Long time behavior

Let us now consider the long time behavior of the system. We first discuss the behavior of the time evolution of the marginal distribution in angle $\tilde{f}(\theta,t)=\int f(\theta,p,t)\,dp$, shown in Fig. 10. For $U=0.55$, the initial condition is Vlasov unstable, thus $\tilde{f}$ drastically changes from $t=1$ to 10 (see Figs. 10(a) and 7). From $t=10$ to 10^4, the distribution is almost frozen and finally relaxes to the equilibrium distribution at $t=10^5$. On the contrary, in the Vlasov stable case, $U=0.69$, (see Fig. 10(b)) the distribution is almost frozen from $t=1$ up to $t=10^3$: *this is the crucial test of the presence of a quasi-stationary state associated to the Vlasov stable initial condition*. Meanwhile, the magnetization $M(t)$ remains constant, well below the equilibrium value. Finally the distribution changes from $t=10^4$ to 10^5, and correspondingly the magnetization $M(t)$ increases to reach equilibrium (similar results have been obtained for Gaussian initial distributions).

In order to characterize the relaxation timescale with respect to the particle number N in the case of the Vlasov stable waterbag initial conditions ($U=0.69$), we have studied the temporal evolution of the magnetization $M(t)$ (a preliminary study has been already reported in Ref. [34]). This can be fitted by the function:

$$M(t)=[1+\tanh(a(N)(\log_{10}t-b(N)))]c(N)+d(N) \tag{58}$$

as shown in Fig. 11(a). The parameters $c(N)$ and $d(N)$ represent the half-width between the initial and the equilibrium levels of $M(t)$ and the initial level of $M(t)$,

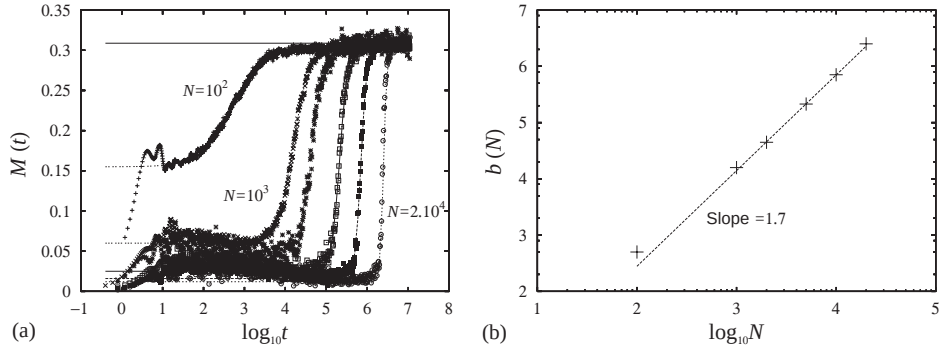

Fig. 11. Panel (a) presents the temporal evolution of the magnetization $M(t)$ for different particles numbers: $N = 10^2(10^3)$, $10^3(10^2)$, $2.10^3(8)$, $5.10^3(8)$, $10^4(8)$ and $2.10^4(4)$ from left to right, the number between brackets corresponding to the number of samples. The horizontal line represents the equilibrium value of M. Panel (b) shows the logarithmic timescale $b(N)$ as a function of N, whereas the dashed line represents the law $10^{b(N)} \sim N^{1.7}$.

respectively (we further comment about such parameters in the appendix). The product $a(N)c(N)$ is the slope at $\log_{10} t = b(N)$, i.e., $a(N)c(N) = \mathrm{d}M/\mathrm{d}(\log_{10} t)|_{\log_{10} t = b(N)}$, and $\tau(N) = 10^{b(N)}$ is the timescale. The most important parameter, $\tau(N)$, presented in Fig. 11(b) as a function of N, is shown to be proportional to $N^{1.7}$. The fit is very good and excludes both the N and the N^2 trivial scalings. This nontrivial power law emerges unexpectedly, since theoretical arguments as well as previous studies of the HMF model suggest trivial divergences of the timescale (typically as N) (see Ref. [3]). Quite interestingly however, Zanette and Montemurro [25] have also investigated the timescale for the HMF model for $U = 0.69$ with a waterbag initial distribution of momenta, but with a fully ordered initial state, i.e., $M(0) = 1$. They have shown that $M(t)$ presents a minimum at t_{min} (already present in the simulation by Latora et al. [11]) which is also proportional to $N^{1.7}$. Although our initial condition is different and hence different scalings could be found, we consider this finding as a confirmation of the presence of nontrivial timescales in the HMF model. Other, apparently unrelated, nontrivial timescales have been found, associated to the vanishing Lyapunov exponent, for instance the well-verified $\frac{1}{3}$ scaling [3].

We were led by this discovery to rescale the momentum distributions $f^*(p,t) = \int f(\theta, p, t)\,\mathrm{d}\theta$ by the nontrivial time-scale $\tau(N) \sim N^{1.7}$, see Fig. 12. The superposition of the curves at different times, in the quasi-stationary state, is quite impressive and we consider this as a strong test of the nontrivial timescale.

There have been recently claims that momentum distributions in quasi-stationary states, obtained from the $M(0) = 1$ initial conditions, could be fitted with single particle distributions inspired by Tsallis statistics [11]. In this study, we could not obtain any reasonable fit of the momentum distribution in Fig. 12 using several values of the Tsallis q parameter with $q > 1$. Moreover, the tails of the distribution are rather sharp, as shown by the inset in lin-log scale, and we can numerically exclude the presence of power law tails.

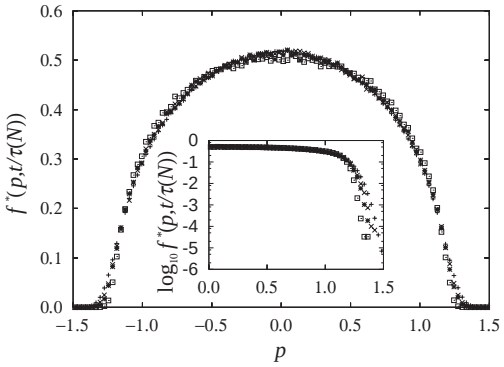

Fig. 12. Temporal evolution of the momentum distribution $f^*(p,t/\tau(N))$ at times rescaled by $N^{1.7}$ for the Vlasov stable case $U = 0.69$: $N = 10^3$ (pluses), $N = 2.10^3$ (crosses), $N = 3.10^3$ (stars) and $N = 10^4$ (open squares). The distributions are plotted for $t/N^{1.7} = 0.0095$, for instance, $t = 6.10^4$ for $N = 10^4$. The four curves, once time-scaled, superpose almost perfectly.

It should be however mentioned that in another physical context, i.e., in the dynamics of self-gravitating N-body systems confined in an adiabatic wall, the long-term time evolution has been argued to sweep through *stellar polytropes*, that are peculiar stationary solutions that maximize Tsallis entropy [35]. However, Chavanis [36], using the minimization of functionals built on conserved quantities (called H-functions in this context), showed that Tsallis entropy can be considered as a particular choice among the infinitely many possible H-functions: their maximization lead to particular stationary solutions of the Vlasov dynamics.

The success of Tsallis statistics in describing quasi-stationary regimes in N-body dynamics remains therefore doubtful. Further studies should fix this puzzling issue.

It should be moreover mentioned that in connection with some aging properties of the $M = 1$ initial state, q-exponential have been used to fit quite efficiently numerical data of correlation functions [37,13].

6. Summary

In this paper we have proposed a general framework, based on Vlasov equation, to study the relaxation to equilibrium of the HMF model. In the short time regime, the behavior of the system is well described by the Vlasov equation, which is a valid approximation for finite times. The stability of the initial conditions is therefore adequately characterized by considering the stability of Vlasov stationary states. We have checked the accuracy of this criterion in comparison with finite N simulations. In addition, a simple analytical derivation of the largest eigenvalue of the linearized Vlasov operator gives an excellent estimate of the numerical timescale in the short time regime of the finite N system.

In the intermediate and long time regimes, two situations have been analyzed separately. The first one, corresponding to unstable stationary Vlasov states, shows a

complex short time evolution before reaching some stationary stable state of the Vlasov equation that is situated close to Boltzmann–Gibbs equilibrium. The latter is finally reached on very long times, $\tau(N) \sim N$. The second one, which begins from Vlasov stable stationary states, evolves through other *quasi-stationary* states that are far from equilibrium and are among the many other stationary Vlasov states. The final relaxation to Boltzmann–Gibbs equilibrium takes place on times that increase with a nontrivial power law in the number of particles $\tau(N) \sim N^{1.7}$. Interestingly, this exponent is consistent with the one recently reported in Ref. [25] for a different initial condition.

We have analyzed the momentum distributions in such a *quasi-stationary* regime and found that they scale properly with the nontrivial exponent. As in Ref. [13], we have been unable to fit the momentum distributions using q-exponentials, as it had instead been done for other initial states in Ref. [11]. This is a negative indication that *quasi-stationary* states can always be described by Tsallis statistics.

An analogy between the slow time evolution appearing in *quasi-stationary* states and the aging phenomenon in glasses and spin-glasses has been proposed in Ref. [37] and further analyzed in Ref. [13]. However, none of these studies has been performed using stationary states of the Vlasov equation as initial conditions. It would be extremely interesting to repeat the study of correlation functions and of other glassy behavior indicators for such states, as already partially done in Ref. [34], where nonstationary stretched exponential correlation functions have been found.

After completing this paper, we became aware of a further, and more complete, study by Choi and Choi [38] of the linear stability of the homogeneous state in both the canonical (Fokker–Planck) and the microcanonical (Vlasov) ensemble. However, this paper does not give any answer to the question of the instabilities caused by the finiteness of the number of particles.

Acknowledgements

We warmly thank F. Baldovin, A. Campa, P.-H. Chavanis, J.-P. Eckman, Y. Elskens, D. Escande, A. Giansanti, V. Latora, M. Nauenberg, A. Rapisarda, F. Tamarit, A. Taruya, C. Tsallis, R. Vallejos, C. Villani for helpful discussions. We also thank P.-H. Chavanis, M. Nauenberg and C. Tsallis for their critical reading of the first version of this manuscript. This work has been partially supported by EU contract No. HPRN-CT-1999-00163 (LOCNET network), the French Ministère de la Recherche grant ACI jeune chercheur-2001 No. 21–31, and the Région Rhône-Alpes for the fellowship No. 01-009261-01. This work is also part of the contract COFIN00 on *Chaos and localization in classical and quantum mechanics* and of the FIRB No. RBNE01CW3M_01 project on synchronization. F.B. is supported by E.U. Network *Stirring and Mixing* (RTN2-2001-00285).

Appendix A. Detailed scaling of the magnetization

Let us recall the fitting function we have used in Section 5.3 for the magnetization $M(t)$

$$M(t) = [1 + \tanh(a(N)(\log_{10} t - b(N)))]c(N) + d(N)\,. \tag{A.1}$$

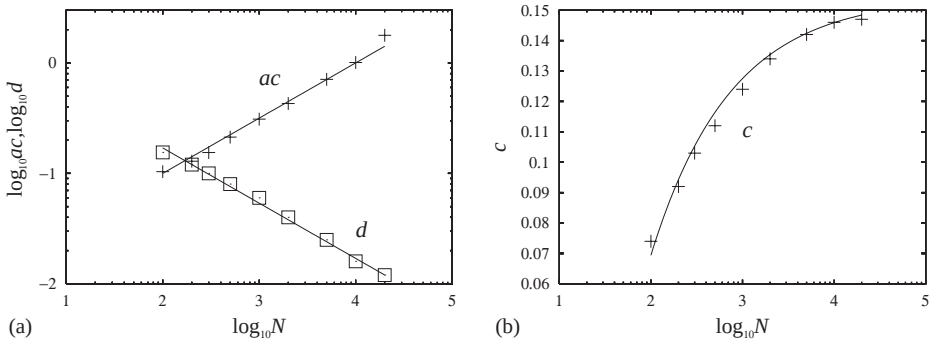

Fig. 13. Log–log plots of parameters $a(N)c(N)$ and $d(N)$ in panel (a), and $c(N)$ in panel (b). The symbols represent numerical results whereas the curves correspond to the fitted functions, given by Eqs. (A.2).

We have already commented about the scaling behavior of $\tau(N) = 10^{b(N)}$. According to Fig. 13, all the parameter set scales as follows:

$$a(N) = \frac{\sqrt{N}}{100c(N)}, \quad 10^{b(N)} = \frac{1}{9}N^{1.7}\,,$$
$$c(N) = \frac{(M_{eq} - d(N))}{2}, \quad d(N) = \frac{1.7}{\sqrt{N}}\,, \tag{A.2}$$

where M_{eq} is the equilibrium level of $M(t)$.

By using the scaling functions (A.2), we can predict when $M(t)$ reaches a given threshold, M_{th}, as a function of N. The corresponding threshold time, t_{th}, with $M(t_{th}) = M_{th}$, has the following expression:

$$t_{th}(M_{th}) = 10^{b}\left(\frac{M_{th} - d}{2c + d - M_{th}}\right)^{\ln 10/2a} = \frac{1}{9}N^{1.7}\left(\frac{M_{th} - \frac{1.7}{\sqrt{N}}}{M_{eq} - M_{th}}\right)^{\ln 10/2a}\,. \tag{A.3}$$

Let us consider, for numerical purposes, two threshold times for both threshold levels, $M_{th} = d + \varepsilon$ and $M_{eq} - \varepsilon$. These two times roughly represent the beginning and ending times when $M(t)$ grows towards the equilibrium value M_{eq} [34]. Numerical results have fluctuations, particularly in the early time region, and hence we have defined $t_{th}(d + \varepsilon)$ and $t_{th}(M_{eq} - \varepsilon)$ as follows:

$$t_{th}(d + \varepsilon) = \max\{t \in R | M(t) < d + \varepsilon\}\,, \tag{A.4}$$

$$t_{th}(M_{eq} - \varepsilon) = \min\{t \in R | M(t) > M_{eq} - \varepsilon\}\,. \tag{A.5}$$

In Fig. 14, the comparison between the numerical results and the theoretical prediction (A.3) for $\varepsilon = 0.0088$ shows an excellent agreement, except in the small N region.

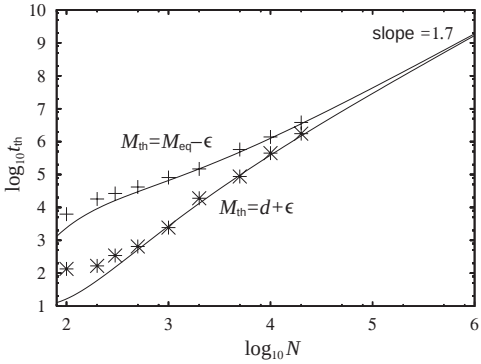

Fig. 14. Dependence of the threshold time $t_{th} = t(M_{th})$ on N for $M_{th} = d + \varepsilon$ (stars) and $M_{th} = M_{eq} - \varepsilon$ (crosses). Both solid curves are obtained from Eq. (A.3).

We remark that both threshold times are approximately proportional to $N^{1.7}$ in the thermodynamic limit. This further confirms the nontrivial scaling law.

References

[1] T. Dauxois, S. Ruffo, E. Arimondo, M. Wilkens (Eds.), Dynamics and Thermodynamics in Systems with Long-range Interactions, Lecture Notes in Physics, Vol. 602, Springer, Berlin, 2002.
[2] A. Campa, A. Giansanti, D. Moroni, Physica A 305 (2002) 137.
[3] T. Dauxois, V. Latora, A. Rapisarda, S. Ruffo, A. Torcini, The Hamiltonian mean field model: from dynamics to statistical mechanics and back, in: T. Dauxois, S. Ruffo, E. Arimondo, M. Wilkens (Eds.), Dynamics and Thermodynamics in Systems with Long-range Interactions, Lecture Notes in Physics, Vol. 602, Springer, Berlin, 2002, also cond-mat/0208456.
[4] S. Inagaki, Prog. Theor. Phys. 30 (1993) 577.
[5] W. Braun, K. Hepp, Commun. Math. Phys. 56 (1977) 101.
[6] H. Spohn, Large Scale Dynamics of Interacting Particles, Springer, Berlin, 1991.
[7] M.-C. Firpo, Étude dynamique et statistique de l'interaction onde-particule, Ph.D. Thesis, Université de Provence, 1999.
[8] M.C. Firpo, Y. Elskens, J. Stat. Phys. 93 (1998) 193.
[9] D. Lynden-Bell, Mon. Not. Roy. Astron. Soc. 136 (1967) 101.
[10] P.H. Chavanis, Statistical mechanics of two-dimensional vortices and stellar systems, in: T. Dauxois, S. Ruffo, E. Arimondo, M. Wilkens (Eds.), Dynamics and Thermodynamics in Systems with Long-range Interactions, Lecture Notes in Physics, Vol. 602, Springer, Berlin, 2002, also cond-mat/0212223.
[11] V. Latora, A. Rapisarda, C. Tsallis, Phys. Rev. E 64 (2001) 056134;
V. Latora, A. Rapisarda, C. Tsallis, Physica A 305 (2002) 129.
[12] C. Tsallis, J. Stat. Phys. 52 (1988) 479.
[13] A. Pluchino, V. Latora, A. Rapisarda, Physica D (2003), in press [cond-mat/0303081], also cond-mat/0306374.
[14] H. Koyama, T. Konishi, Phys. Lett. A 279 (2001) 226;
B.N. Miller, J.L. Rouet, Phys. Rev. E 65 (2001) 056121;
T. Tatekawa, K. Maeda, The Astrophys. J. 547 (2001) 531.
[15] S. Chandrasekhar, Rev. Mod. Phys. 15 (1943) 1.
[16] M. Antoni, S. Ruffo, Phys. Rev. E 52 (1995) 2361.
[17] J. Barré, Mécanique statistique et dynamique hors équilibre de systèmes avec intéractions à longues portées, Ph.D. Thesis, ENS, Lyon, 2003.

[18] J. Barré, F. Bouchet, T. Dauxois, S. Ruffo, Large deviation techniques applied to long-range interacting systems, in preparation.
[19] V. Latora, A. Rapisarda, S. Ruffo, Phys. Rev. Lett. 80 (1998) 692.
[20] V. Latora, A. Rapisarda, S. Ruffo, Phys. Rev. Lett. 83 (1999) 2104;
V. Latora, A. Rapisarda, S. Ruffo, Physica A 280 (2000) 81.
[21] V. Latora, A. Rapisarda, S. Ruffo, Physica D 131 (1999) 38.
[22] V. Latora, A. Rapisarda, Nucl. Phys. A 681 (2001) 331c.
[23] V.I. Arnold, Izv. Vyssh. Uchebn. Zaved. Mat. 54 (5) (1966) 3–5 (Engl. transl.: Am. Math. Soc. Trans.).
[24] D.D. Holm, J.E. Marsden, T. Ratiu, A. Weinstein, Phys. Rep. 123 (1985) 1.
[25] D.H. Zanette, M.A. Montemurro, Phys. Rev. E 67 (2003) 031105.
[26] F. Bouchet, The stochastic process of equilibrium fluctuations of a system with long-range interactions, cond-mat/0305171.
[27] R. Robert, J. Sommeria, J. Fluid. Mech. 229 (1991) 291.
[28] J. Miller, Phys. Rev. Lett. 65 (1990) 2137.
[29] D. Lynden Bell, Mon. Not. Roy. Astron. Soc. 136 (1967) 101.
[30] P.H. Chavanis, Ann. N. Y. Acad. Sci. 867 (1998) 120;
P.H. Chavanis, J. Sommeria, R. Robert, Astrophys. J. 471 (1996) 385.
[31] S. Inagaki, T. Konishi, Publ. Astron. Soc. Japan 4 (1993) 733.
[32] R.I. McLachlan, P. Atela, Nonlinearity 5 (1992) 541.
[33] H. Yoshida, Celestial Mechanics and Dynamical Astronomy 56 (1993) 27–43.
[34] Y.Y. Yamaguchi, Phys. Rev. E 68 (2003) 066210.
[35] A. Taruya, M. Sakagami, Phys. Rev. Lett. 90 (2003) 181101, and references therein.
[36] P.H. Chavanis, Phys. Rev. E 68 (2003) 036108.
[37] M.A. Montemurro, F.A. Tamarit, C. Anteneodo, Phys. Rev. E 67 (2003) 031106.
[38] M.Y. Choi, J. Choi, Phys. Rev. Lett. 91 (2003) 124101.